NUMERICAL SIMULATION OF THE HIGH-LATITUDE NON-STATIONARY IONOSPHERIC ALFVÉN RESONATOR DURING AN IPDP EVENT

K. PRIKNER[1], K. MURSULA[2], J. KANGAS[3], F. Z. FEYGIN[4], AND R. KERTTULA[2]

ABSTRACT

The ionospheric Alfvén resonator (IAR) was numerically simulated under non-stationary ionospheric and magnetospheric conditions of the IPDP event of December 4, 1986. The full numerical wave method was applied using height profiles of the ionospheric plasma parameters obtained from the Scandinavian EISCAT radar measurements close to the Ivalo latitude. An attempt to model the inverse problem of numerical simulation – prolongation of the electron density profiles at altitudes above the ionospheric F layer – was made on the basis of the IAR simulation in correlation with the IPDP frequency increase. The change of the IAR wave characteristics during the substorm was illustrated by height profiles of the total wave amplitude and various polarization characteristics, taking into consideration the ordinary L-mode and the extraordinary R-mode waves for parallel and non-parallel incidence with respect to the magnetic field line.

Keywords: Pc1 pulsations, IPDP pulsations, Ionospheric Alfvén Resonator, fundamental frequency window, EISCAT measurements.

1. INTRODUCTION

The idea of the ionospheric Alfvén resonator (IAR) has been developed since the 1960's (*Greifinger and Greifinger, 1968*; *Fujita, 1987*) in connection with investigating different ionospheric waveguide phenomena. The IAR is centred around the F-layer electron density maximum and affects hydromagnetic wave frequencies between ~ 0.1 and 10 Hz. The IAR was further developed by the Russian group (*Polyakov and Rapoport, 1981*; *Belyaev et al., 1989*; *Trakhtengerts et al., 2000*) in introducing the Alfvén maser theory (*Belyaev et al., 1985*). The wave phenomena observed on the ground provide a possibility of deriving the basic IAR parameters. In turn, these IAR parameters

1 Geophysical Institute, Academy of Sciences of the Czech Republic, Boční II, 14131 Praha 4 - Spořilov, Czech Republic (e-mail: kpr@ig.cas.cz)

2 Department of Physics, University of Oulu, P.O. Box 3000, FIN-90014 Oulu, Finland (e-mail: Kalevi.Mursula@oulu.fi; Raine.Kerttula@oulu.fi)

3 Sodankylä Geophysical Observatory, University of Oulu, FIN-99600 Sodankylä, Finland (e-mail: Jorma.Kangas@sgo.fi)

4 United Institute of Physics of the Earth, Russian Academy of Sciences, Bolshaya Gruzinskaya 10, 123810 Moscow, Russia (e-mail: Feygin@uipe-ras.scgis.ru)

may provide information on ionospheric plasma parameters. Thus IAR can be used as a tool for ionospheric plasma diagnostics (*Prikner et al., 1996*).

The first studies of the IAR spectral resonance structures (SRS) were made at middle latitudes (*Belyaev et al., 1989*; *Belyaev et al., 1990)* and later at high latitudes (*Lysak, 1991, 1993*; *Belyaev et al., 1999*; *Demekhov et al., 2000*). The intimate relationship between the Pc1 frequency and the fundamental IAR frequency has been explored in a series of papers (see, e.g., *Demekhov et al., 1994; Mursula et al., 2000*). The subauroral and auroral regions of the ionosphere are frequently excited by broadband and impulsive EMIC-waves of magnetospheric origin. Continuous Pc1 pearls are typical of quiet IAR conditions. During substorm intervals with intensive precipitation of hot particles into the ionosphere, the ionospheric disturbance can lead to a non-stationary IAR above a ground observation point.

Hitherto the magnetospheric generation mechanism of IPDP pulsations (intervals of pulsations with diminishing period) predominated (*Heacock, 1973*; *Kangas et al., 1974*; *Gul'elmi, 1974*; *Koleszar, 1989*). *Kleimenova et al. (1995)* found a systematic connection between the occurrence of IPDP pulsations and the ionospheric trough above the observation point. The trough often extends to lower latitudes during substorm development. *Mursula et al. (2000)* and *Prikner et al. (2000)* presented a relationship between the frequency characteristics of a structured IPDP event and the numerically simulated non-stationary IAR. Using EISCAT incoherent scatter radar measurements of the various ionospheric plasma parameters (electron density, electron temperature, ion temperature, effective ion mass and collision frequency) extended at best up to 600 km and extrapolated up to 1000 km, a 'full wave analysis' was applied over a substantial altitude extent of the IAR.

In *Mursula et al. (2000)* the instantaneous central frequency of the IPDP event was identified with the simulated fundamental IAR frequency[#]. The frequencies increased during non-stationary substorm conditions, and a simultaneous inward motion of the wave source region was observed. This leads to the conclusion that the non-stationary ionospheric plasma conditions during substorms lead to an increase of the IAR fundamental frequency. The development of the IPDP signal on the ground during the substorm was related to the inward motion of the EMIC-wave source to lower L-shells and simultaneous changes in the ionosphere (*Mursula et al., 2000*). Thus it is most probable that both the magnetospheric and ionospheric (IAR) aspects must be taken into account in IPDP generation and formation of the ground signal.

The IAR controls the signal observed in the ionosphere and on the ground (*Prikner et al., 2001*). According to our scenario the IPDP can be observed on the ground if the increasing EMIC-wave frequency during the inward motion of the wave source region coincides with an increase of the fundamental IAR frequency. The peak of the amplitude transmission coefficient at the fundamental IAR frequency forms the frequency window for transmitting an EMIC-wave signal to the ground. A variance between the EMIC-wave

---

[#] By the term 'fundamental frequency' of the IAR we shall hereinafter understand the central frequency peak of the horizontal amplitude transmission coefficient through the IAR simulation domain (ionospheric layer up to an altitude of 1000 km), however, 'eigenfrequencies' of a resonator are defined on the basis of the energy stored in the resonator, and may or may not exactly coincide with maxima of the transmission coefficient.

spectrum and the IAR frequency window causes the extinction of the signal on the ground.

The proposed mechanism of the IPDP formation in the IAR needs further experimental support and verification by more IPDP events. *Prikner et al. (2000)* presented height profiles of several wave characteristics at the fundamental IAR frequency during a structured IPDP event, using the incidence of an L-polarized Alfvén wave only upon the ionosphere at a height of 1000 km and under field-aligned propagation only.

The purpose of this paper is, among others, to attempt to model the inverse problem on the basis of the IAR ground fundamental frequency response - prolongation of the $N_e(z)$ profiles above the ionospheric F layer where EISCAT data are missing. This paper presents numerically simulated plasma height profiles of the IAR above the EISCAT radar range during the IPDP event of December 4, 1986. An unstructured IPDP event was observed by the latitudinal chain of Finnish search-coil magnetometers. We give examples of simulated total wave height structures (both the $\boldsymbol{E}$- and $\boldsymbol{B}$-fields), corresponding to different incidence angles and both L- and R-mode incident waves (the ordinary Alfvén and the extraordinary isotropic wave, respectively).

EMIC-waves propagating to the ionosphere largely consist of the Alfvenic L-mode waves guided along magnetic field lines. But inside the IAR the R-modes generated by intermodal coupling play an important part (transformation to the horizontally propagating waveguide modes). The „simulation domain" used (up to a level of 1000 km) is the main part of the IAR with respect to the fundamental resonance frequency. The whole IAR domain extends up to ~3000 km below the Alfvén velocity maximum. R-modes generated inside the upper IAR region and propagating downwards can also play a role in resonances in the simulation domain. Thus it would be interesting to know the characteristics of an R-mode wave. An intermodal coupling of the incident L- and R-modes on the simulation domain can affect the resulting total wave altitude structure. We can obtain a more comprehensive idea of the altitude structure of the IAR total wave at the fundamental frequency and its change during the present non-stationary substorm conditions.

2. OBSERVATIONS

The IPDP event of 4 December 1986 between 19:00 UT and 20:30 UT was recorded over the entire Finnish latitudinal chain of induction magnetometers (Kevo, Ivalo, Sodankylä, Rovaniemi, Oulu and Nurmijärvi). The IPDP event developed slowly and was mostly unstructured, with a few pearl packets at the end of the event at about 20:20 UT only. This IPDP event was previously studied by *Kangas et al. (1988)*. It was found that the measured electric field could explain the frequency change due to the radial $\boldsymbol{E} \times \boldsymbol{B}$ drift of substorm injected protons. Here the attention will be focused on the possible role of the non-stationary IAR to form the IPDP spectrum.

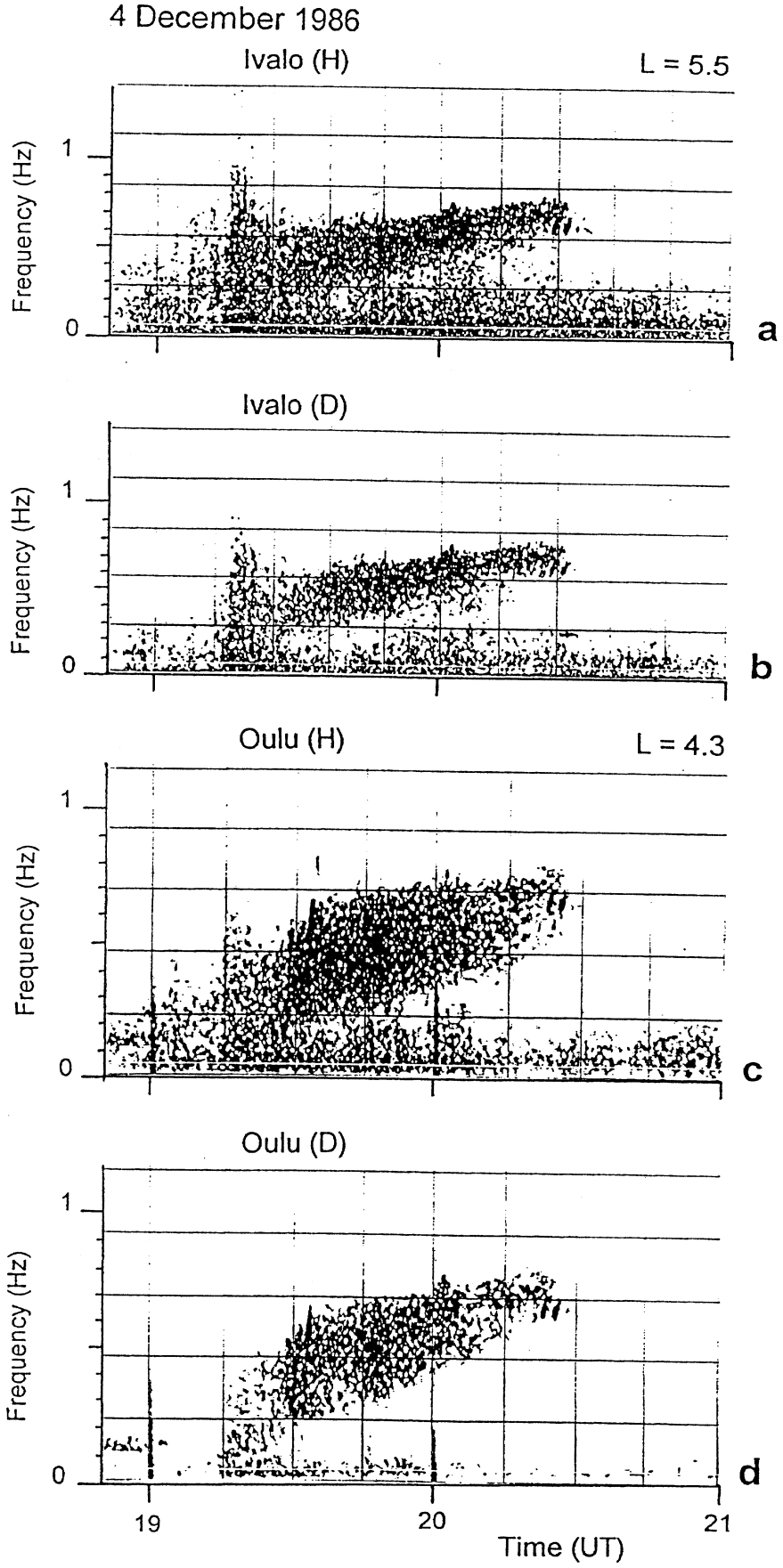

Fig. 1. The signal dynamic spectra of the IPDP event on 4 December 1986, a) and b) at Ivalo, c) and d) at Oulu, Finland: H (meridional, N-S) and D (E-W) components.

An intense IPDP event was observed over a wide latitude region as shown in Fig. 1. The signal was intense in both the H (N-S) and D (E-W) components during the whole event, e.g., at Ivalo (geogr. coordinates: $\phi = 68.55$ N, $\lambda = 27.28$ E, corr. geomag. coordinates: $\Phi = 65.0$ N, $\Lambda = 109.3$ E; $L \approx 5.5$) in Fig. 1. Moreover, a broad-band burst of PiB pulsations observed at Ivalo at about 19:15 UT is a manifestation of the substorm onset with particle precipitation into the local ionosphere. At lower latitudes (Sodankylä, Oulu) the PiB signal was not observed. At a higher latitude station Kevo ($L = 6.1$, $\phi = 69.75$ N, $\lambda = 27.02$ E) both the signals were nearly invisible.

The substorm started under relatively quiet geomagnetic conditions (the preceding activity was characterized by $K_p \approx 1_0 - 2_0$; during the event $K_p = 2_+$). We estimate that the source field lines of the observed IPDP pulsation were close to the Ivalo latitude, where the PiB burst was distinctly observed. The intensity of the H-component at Oulu was higher than that of the D-component indicating a possibility of ducting of compressional waves in the meridional direction (*Lysak, 1999*).

The EISCAT radar was operating at the CP-3 mode during the IPDP interval. This mode provides measurements of the latitudinal profile of ionospheric parameters. For the present version a 15-position scan was used resulting in a geographic latitude coverage of 64.2°N to 74.2°N at an altitude of 325 km along the magnetic meridian. At higher altitudes the plasma height profiles have to be numerically modelled in order to yield an IAR fundamental frequency, i.e. a transmission coefficient peak value fitting the central IPDP frequency (*Mursula et al., 2000*, and *Prikner et al., 2000*).

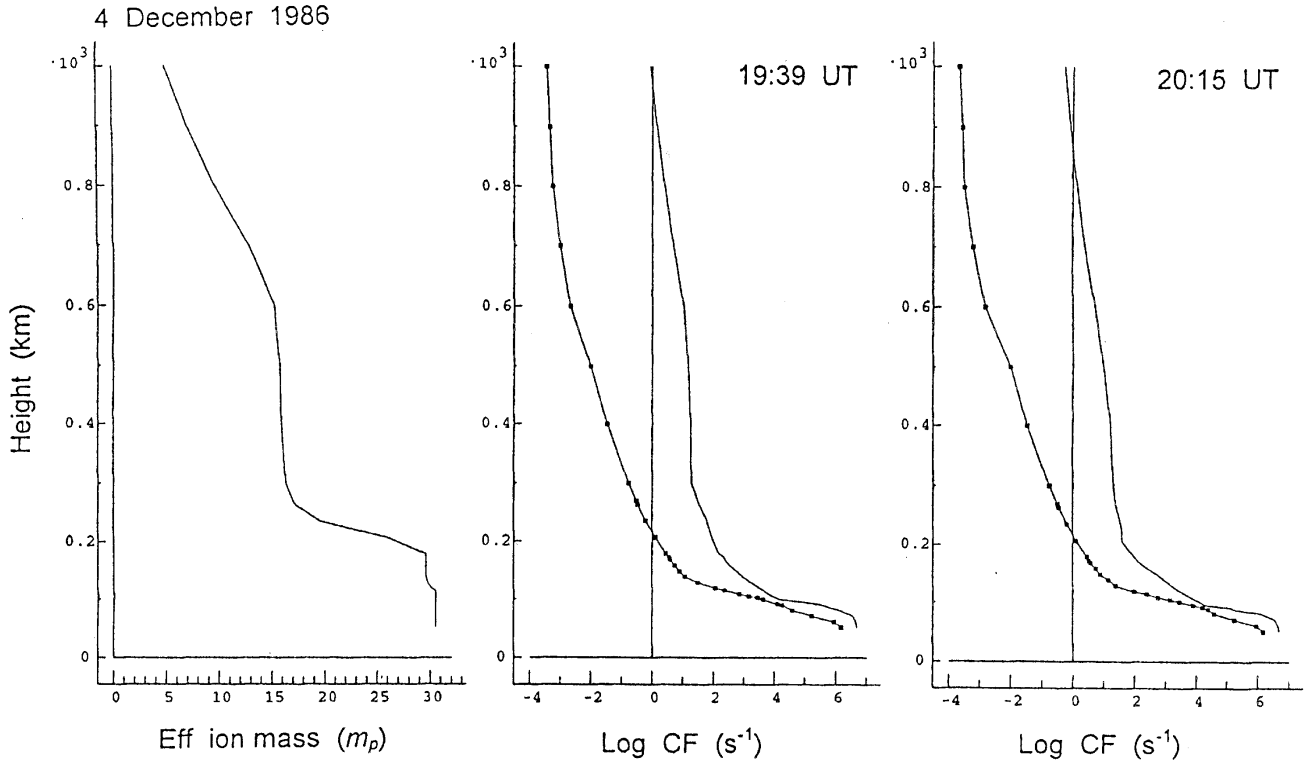

Fig. 2. The height profiles of the effective ion mass (in proton mass units), and the electron (smooth line) and ion (line with squares) collision frequencies during the two selected time sections of IPDP.

The EISCAT data fix the height profiles of electron density, electron and ion temperature, effective electron-ion and ion-neutral collision frequencies up to an altitude of 325 km. A decrease of the electron density in the ionosphere with a constant log – scale direction factor above the F-layer has been assumed. The numerical process according to *Prikner (1986)* and mentioned in *Prikner et al. (2000)* was used to construct the height profiles of the effective electron and ion collision frequencies up to an altitude of 1000 km (also see *Prikner et al., 2001*). A prevailing NO^+ and O_2^+ ion content was assumed for $z < 150$ km, and O^+ ions at higher altitudes up to 600 km. Even higher, and in the winter night ionosphere, predominance of H^+ ions was assumed near the top of the considered ionosphere domain at $z_{max} = 1000$ km (*Krinberg and Taschilin, 1984*). The height profiles of the effective particle collision frequencies (ν_e, ν_i) and the effective ion mass used in the model are shown in Fig. 2 for two selected time intervals.

3. THE NUMERICAL SIMULATION METHOD

The principles of the numerical simulation method applied here were described in a series of papers, among others in *Prikner et al. (2000)*. The matrix method is presented in *Vagner (1982)*, *Prikner and Vagner (1983, 1991)* and *Vagner and Prikner (1983)*.

The simulation input data are:

a) Characteristics of the plasma medium: Realistic height profiles of electron density, ion effective mass and effective electron and ion collision frequencies. The ionosphere is represented by a thin plane structure (optimal ionospheric stratification was found for $\Delta z = 10$ km) in an external dipole magnetic field $\boldsymbol{B}_E(z)$ with the dipole magnetic field moment $M_E = 8.17 \times 10^{22}$ A m^2. The assumed thickness (height) of the ionospheric resonator is $z_{max} = 1000$ km. The neutral atmosphere is 50 km thick and the conductivity of the Earth's surface is taken to be homogeneous with the specific value $\sigma_E = 10^{-2}$ S/m.

b) Wave propagation characteristics: Polarization of the incident homogeneous plane wave (L- or R-polarization; ordinary Alfvén L-wave rotates counterclockwise looking along $\boldsymbol{B}_E$-field), frequency f, orientation of the wave vector $\boldsymbol{k}$ with respect to $\boldsymbol{B}_E(z)$ in the magnetic meridional plane. The inclination α_E of $\boldsymbol{B}_E(z)$ is taken to be constant above the ground observation point (a feature of the dipole field along the radial direction) and negative in the northern hemisphere. Assuming parallel incidence, $\boldsymbol{k} \| \boldsymbol{B}_E$, the incidence angle with respect to the horizontal plane, β, is then $\beta_{\|} = -\alpha_E$ in the northern hemisphere.

In this paper we will only briefly describe the output local wave characteristics obtained by simulation. A more detailed presentation can be found in the above mentioned papers. The total wave field at any ionospheric height, at its boundary and on the ground is determined by a 4×4 matrix method and it is a function of frequency f and height z :

a) The normalized real horizontal wave amplitudes B_{hor} and E_{hor} at frequency f and height z are defined as the ratio between the real horizontal amplitude, e.g., for the magnetic field component,

$$ {}^{(B)}A_{hor}(f,z)_{(L,R)} = \sqrt{|B_x(f,z)|^2 + |B_y(f,z)|^2}_{(L,R)} , \qquad (1) $$

and the amplitude of the wave incident upon the upper boundary of the simulation domain at height $z = z_{max}$ as follows:

$$ Norm\,{}^{(B)}A_{hor}(f,z)_{(L,R)} = {}^{(B)}A_{hor}(f,z)_{(L,R)} / {}^{(B)}A^{(inc)}_{hor}(f, z = z_{\max})_{(L,R)} . \qquad (2) $$

B_x and B_y are the horizontal components of the complex total wave amplitude provided by computations. This ratio on the ground surface at $(z = 0)$ is the normalized transmitted amplitude of the wave B-field horizontal component (*wave magnetic field transmission coefficient*),

$$ {}^{(B)}T_{hor}(f)_{(L,R)} = {}^{(B)}A_{hor}(f, z = 0)_{(L,R)} / {}^{(B)}A^{(inc)}_{hor}(f, z = z_{\max})_{(L,R)} , \qquad (3) $$

b) According to the method described by *Vagner and Prikner (1983)*, the *polarization properties* (the sense of rotation, ellipticity of the polarization ellipse defined as the ratio of the minor and major axes, *b/a*, and deflection of the major axis from the magnetic field meridian plane) can be determined at any height for the total $\boldsymbol{B}$ and $\boldsymbol{E}$ wave fields.

It should be noted that the plane-wave calculations applied here can be used to interpret the EMIC-wave packets with transverse size comparable to or larger than the wavelength of the magnetosonic (R) wave modes. If the packets are of a smaller width, the polarization features will be significantly different. This parameter is difficult to judge in the particular event studied here. However, the simulated frequency – amplitude characteristics match the observed characteristics of the signal well. We assume a sufficient transverse size of the EMIC-wave packets in the present case.

4. MODELLED IAR FREQUENCIES

We first study the change of the vertical profiles of plasma properties during the IPDP development at Ivalo displayed in Fig. 1. Nine profiles have been selected for processing. For two of them the height profiles of the electron and ion effective collision frequencies are shown in Fig. 2, together with the profile of the effective ion mass which is assumed stable (*Krinberg and Taschilin, 1984*). In order to model the time variation of the basic IAR characteristic, the electron density $N_e(z)$, recursive computations were carried out varying the $N_e(z)$-profile at $z > 300$ km. The profiles agree with the EISCAT data at $z < 320$ km. Coincidence between the modelled IAR fundamental resonance frequency and the simultaneous IPDP frequency was required. The modelled $N_e(z)$-profiles corresponding to the nine time intervals for Ivalo are depicted in Fig. 3. The modelled values above the ionospheric F layer are within the range of the realistic values of many different ionosphere profiles measured by the EISCAT CP-1 vertical mode (measurements provided data up to an altitude of 600 km). Measurements of the CP-1 mode at Tromsö correspond enough to the Ivalo latitude. During the IPDP development the N_e-values ranged from 10^{10} to 10^9 electron/m^3 at the boundary of the IAR simulation domain at $z_{max} = 1000$ km. This agrees well with the previously analysed ionosphere models, as in

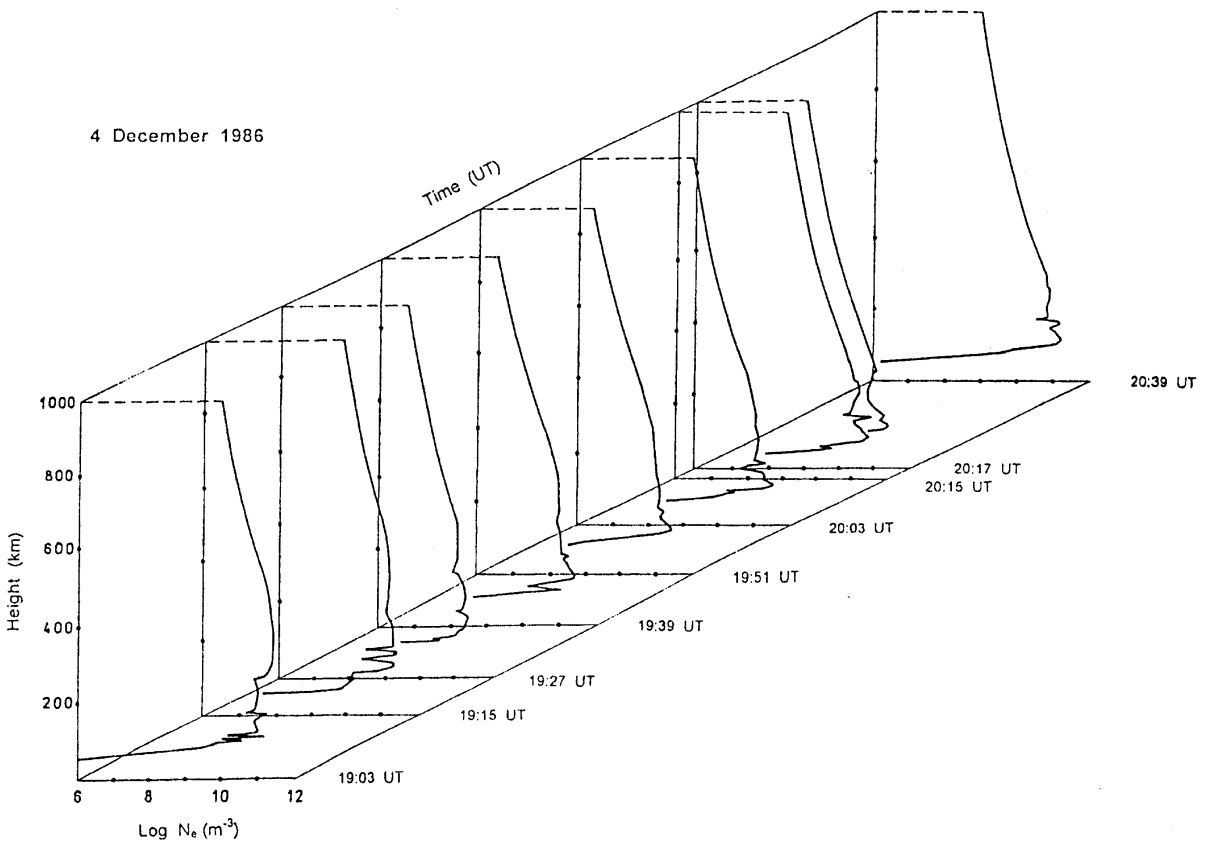

Fig. 3. The N_e height profiles during the nine selected time sections before and during the IPDP development, modelled for Ivalo. At heights below 300 km, the EISCAT measurements were matched.

Prikner and Vagner (1990). Very good agreement was found also with the models developed by *Prikner (1986)* and models for the winter season constructed on the basis of modelling by *Krinberg and Taschilin (1984).*

We assume $\boldsymbol{B}_E$-parallel incidence at $z_{max} = 1000$ km, and inclination $\alpha_E = -76$ deg. The corresponding time development of the frequency spectra of transmission coefficient ${}^{(B)}T_{hor}(f)$ (eq. 3) for the wave horizontal magnetic field is shown in Fig. 4 in the case of the incident L-mode wave. As seen in Fig. 4 the spectral width of the IAR fundamental frequency ($\Delta f \sim 0.3 - 0.4$ Hz) and that of the IPDP at Ivalo (Fig. 1a) correspond with one another fairly well. Also, the IAR fundamental frequency increases in time following the frequency rise of IPDP.

Our experience in the numerical modelling of the IAR amplitude transmission coefficient peaks and their frequency shifts with respect to the N_e-height profile variations reveals some general dependences:

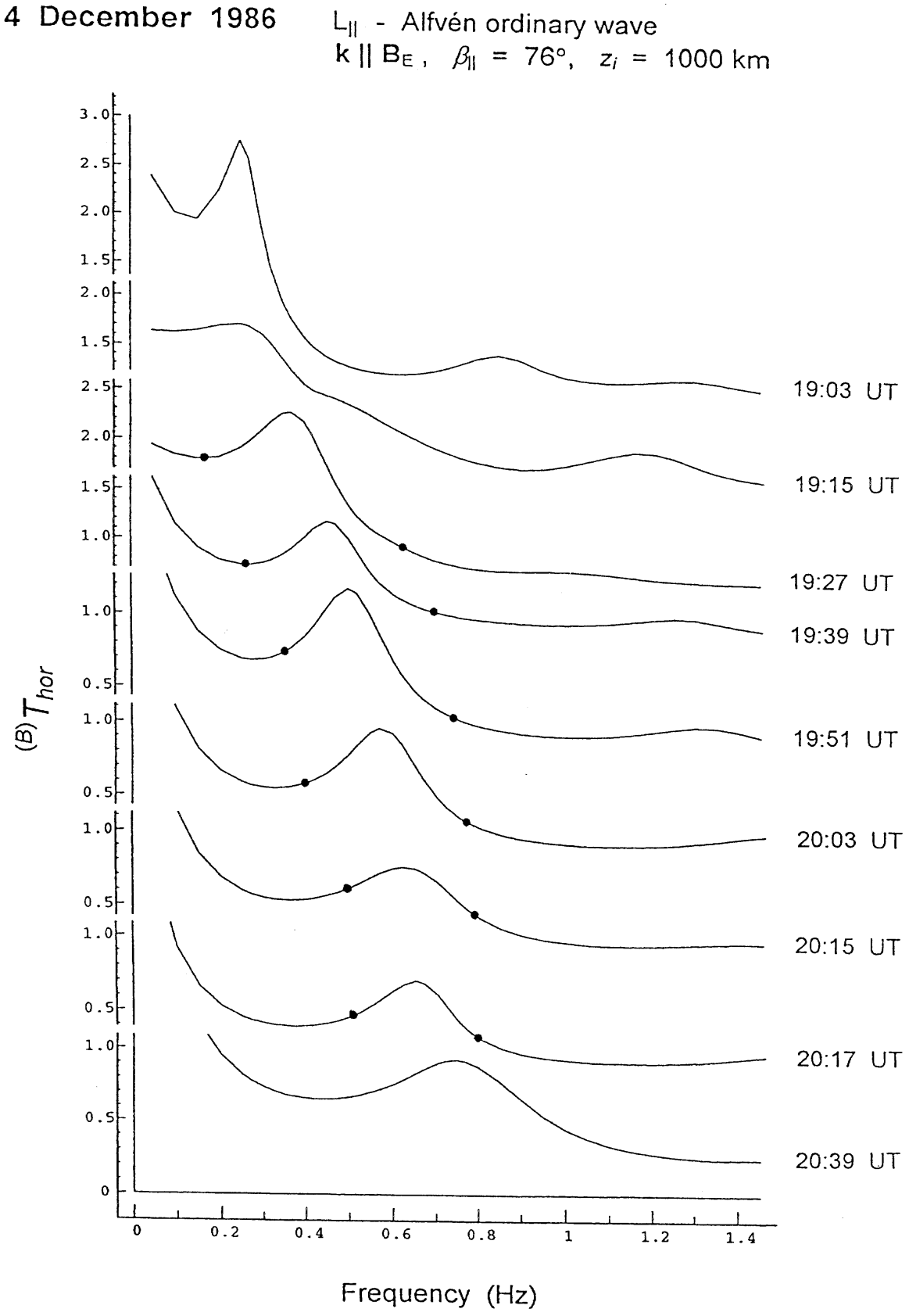

Fig. 4. The frequency spectra of the normalized transmitted magnetic horizontal amplitude (amplitude transmission coefficient) for the nine time sections of IPDP, using the $N_e(z)$-profiles of Fig. 3. The marks denote the widths of the IPDP frequency range in Fig. 1a.

High values of N_e in the quiet subauroral ionospheric F region (the midday quiet ionosphere conditions) lead to very low IAR fundamental frequencies (frequently below the Pc1 range of frequencies, at $f < 0.2$ Hz). Lower N_e values in the quiet ionospheric F region (the local evening or morning quiet ionosphere) with the smooth exponential decrease above the F-maximum lead to higher values of the IAR fundamental frequency, matching the Pc1 range of frequencies. IPDPs mostly occur in the late afternoon and evening hours.

The disturbed subauroral ionosphere with sweeping out of plasma from above the F layer and occasional increase of N_e in the E-F1 region (substorms with an extending ionospheric trough, see *Bauske et al., 1997*) lead to a decrease of effective IAR dimensions and to a pronounced and fast increase of the IAR fundamental frequency. These are the conditions for observation of IPDP if the magnetospheric mechanism of the EMIC-wave generation is also activated. Smooth variations of the upper ionosphere plasma concentration above the F layer lead to a smooth and slow variation of the IAR frequency window. If an EMIC-wave signal matches the window, a Pc1 signal with smooth frequency shifts can be observed on the ground (*Prikner et al., 2001*). A steeper height decrease of N_e yields slightly higher frequencies, a slower decrease slightly lower IAR fundamental frequencies.

The required $N_e(z)$ height profiles of Fig. 3 show a continuous decrease of N_e in time at heights above $z > 200$ km. The EISCAT data indicated a small but sporadic increase of N_e in the lower ionosphere (E-region, $z < 150$ km) in accordance with *Bauske et al. (1997)*. Such a $N_e(z)$-profile variation is in accordance with the development of the ionospheric trough above Ivalo during the IPDP event (*Kleimenova et al., 1995*).

The broad-band burst of pulsations at 19:15 UT at Ivalo (Fig. 1) was a PiB pulsation signal. The IPDP frequency rise started thereafter. This type of pulsation usually indicates a substorm onset phase with intensive ULF waves and particle precipitation into the auroral and subauroral ionosphere. IPDPs frequently follow this onset. Note that the EISCAT N_e-height profile during the hot proton penetration at this time leads to a breakdown of the modelled IAR L-resonance (see Fig. 4). The $N_e(z)$-values (Fig 3) fluctuated by one order of magnitude (between 2.5×10^{10} and 2.5×10^{11} m^{-3}) in a narrow altitude range in the lower ionosphere above 100 km. Thus, the PiB disturbance coincided with the strong perturbance of the E – F1 region. This region plays an important part in the IAR as the bottom high conductive mirroring layer of the resonator. The splitting of this region during the substorm onset and particle precipitations can break down the IAR action, and broad-band primary EMIC waves can penetrate through the disrupted resonator to the ground (the frequency window filtration breaks down). A wide frequency range of observed signals can be expected during a sudden disturbance, accompanied by a strong particle penetration into the ionosphere.

The IAR frequency window could be formed once again around the transmission coefficient peak later when conditions in the E – F1 region become settled. Then the IAR ability to modulate transmitting signals could be restored and a narrower frequency band of the IPDP signal could be observed on the ground. The IPDP forming in the IAR has to conform also with the magnetospheric mechanism of wave packet generation – well developed IPDP can be observed on the ground only if the EMIC-wave packet matches the IAR frequency window, i.e. if ionospheric plasma variation follows the EMIC-wave spectrum variation. Perhaps that is why IPDPs are not observed more frequently.

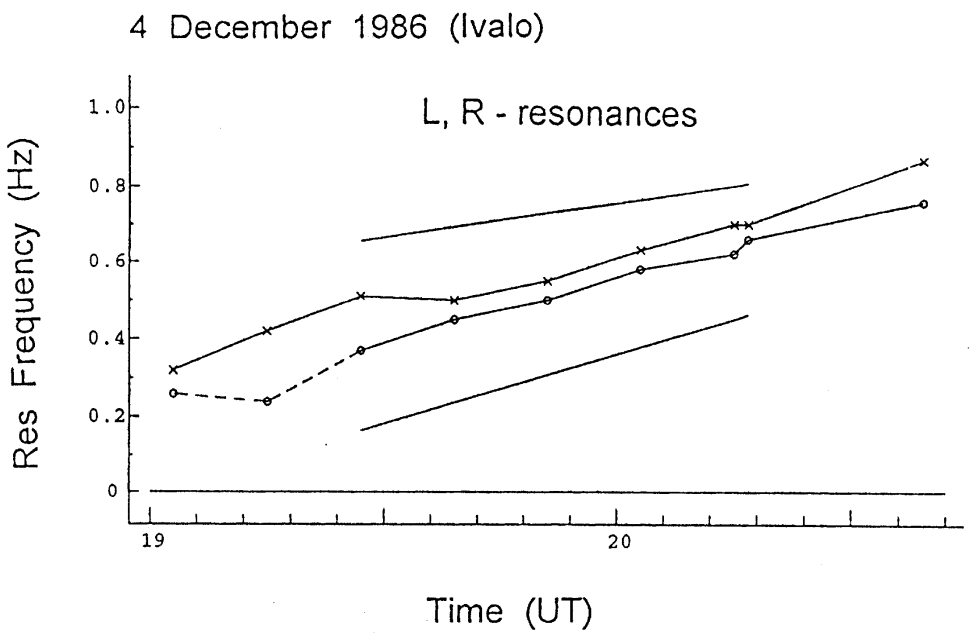

Fig. 5. Time variation of the modelled fundamental L- and R-mode resonance frequencies compared with the frequency increase during the IPDP event at Ivalo ($L_{||}$-wave resonances marked 'o', and $R_{||}$-wave resonances '×').

The fundamental resonance peak frequencies computed for the Ivalo N_e-profiles (Fig. 3) are shown in Fig. 5 for both $L_{||}$-mode (marked 'o') and $R_{||}$-mode waves (marked '×') during the nine time sections (|| stands for $\boldsymbol{B}_E$-parallel incidence). The straight lines depict the limits of the IPDP frequency band variation taken from Fig. 1a. The value related to the total $L_{||}$-wave resonance at 19:15 UT is only approximate during the PiB disturbance of the IAR. The $R_{||}$-wave resonance was more apparent at this time. Fig. 5 shows that the fundamental $R_{||}$-mode resonance frequency is systematically slightly higher than the $L_{||}$-mode resonance frequency. The R-mode waves propagate isotropically, contrary to the L-mode waves which are guided along the magnetic field lines. Thus, the effective IAR dimension tends to be shorter under vertical propagation for the R-mode than for the field-line-guided L-mode. Note, however, that both resonance frequencies lie within the IPDP frequency band, but the L-wave is the central guiding wave.

5. HEIGHT PROFILES OF IAR RESONANCE CHARACTERISTICS

Total waves generated by the incident parallel $L_{||}$- and $R_{||}$-mode waves ($\beta_{||} = 76°$) at fundamental resonance frequencies have been calculated along the whole IAR height profile. As seen above, the fundamental resonance frequencies differ slightly between the two wave modes. At 19:39 UT they are $f_{res}{}^{L} = 0.45$ Hz and $f_{res}{}^{R} = 0.50$ Hz, and at 20:15 UT $f_{res}{}^{L} = 0.62$ Hz and $f_{res}{}^{R} = 0.70$ Hz. The same resonance frequencies have been determined for the non-parallel incidence angle $\beta = 70°$. Thus, the fundamental IAR resonance frequency is quite stable over a fairly wide range of meridional incidence angles.

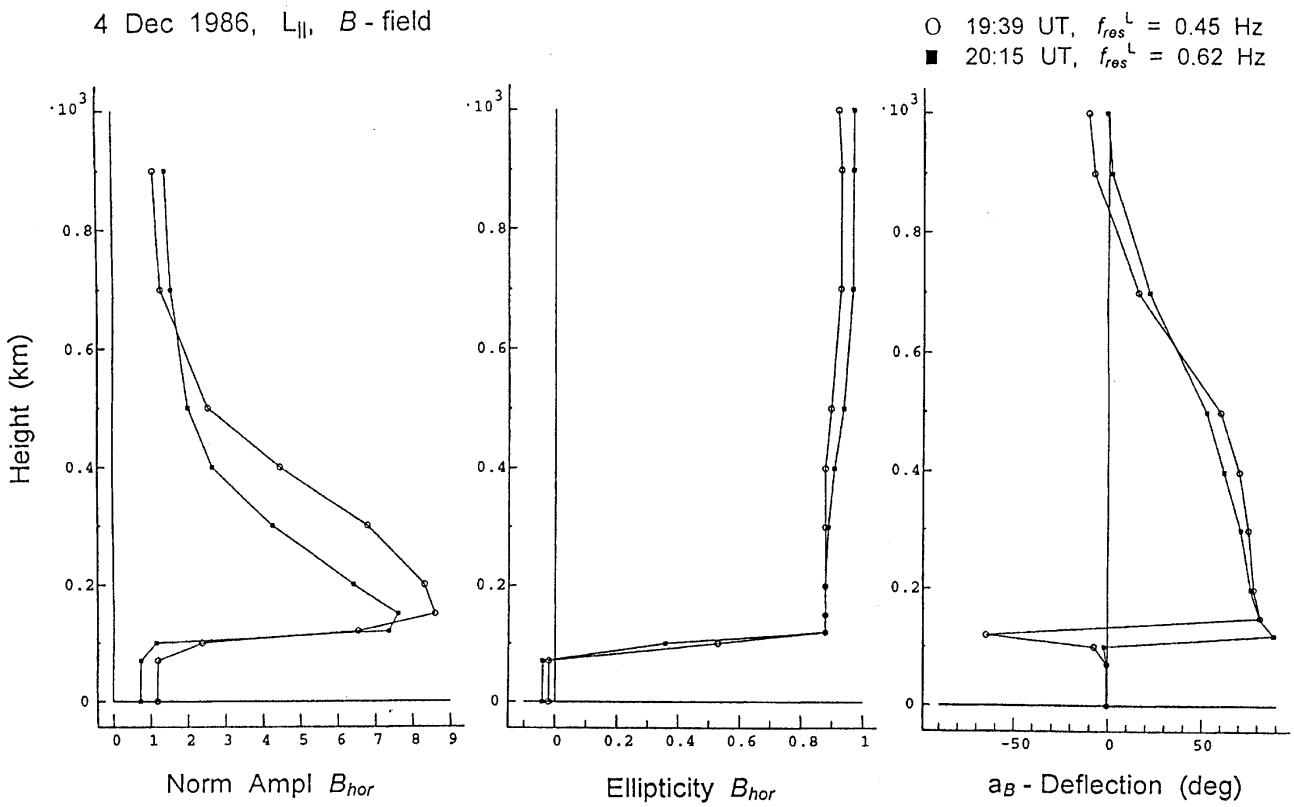

Fig. 6. Height profiles of the normalized B_{hor}-field amplitude, polarization ellipticity and the a_B-deflection angle (positive angles indicate deflection to the east from the north) at the two selected time sections of IPDP for an incident $L_{||}$-wave. (Positive ellipticity values indicate L-polarization in the horizontal plane).

The height profiles of the normalized total B_{hor}-field amplitude (eq. 2), ellipticity of the B_{hor}-polarization ellipse and deflection of its major a_B-axis from the magnetic meridian plane are depicted in Fig. 6 for parallel incidence at 19:30 UT and 20:15 UT (considering a sufficient transverse size of the EMIC-wave packets as was mentioned above in Sect. 3). During the IPDP development the height of the resonator amplitude maximum (Fig. 6) decreased by a few tens of km, corresponding to the increase of the IAR fundamental frequency (Fig. 4). The height range of the B_{hor}-wave field amplification in the IAR is between 100 km and 600 km. This range decreased with the trough development and increasing IPDP frequency. The B_{hor}-polarization of the $L_{||}$-wave is nearly circular over the whole height profile. After transition through the E-layer, below 100 km the B_{hor}-polarization quickly turns into roughly linear with a small R-sense dominance. The a_B-deflection is transverse to the magnetic meridian (NE-SW direction) inside the main IAR. Below the E-F1 layer the main axis rotates into the magnetic meridian plane due to the Hall conductivity (*Nishida, 1964*; *Hughes, 1974*).

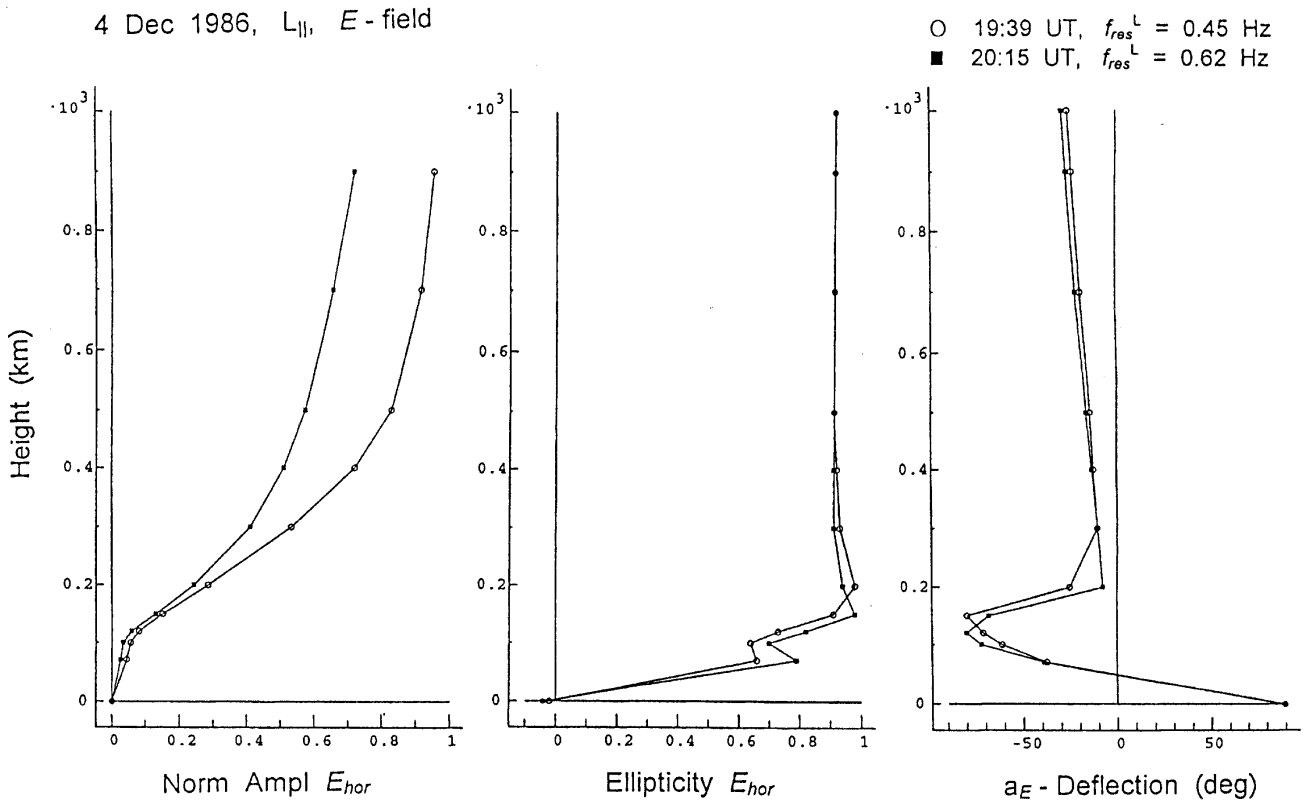

Fig. 7. The same profiles as in Fig. 6, but for the E_{hor}-field.

In Fig. 7 the same height profiles are depicted for the normalized E_{hor}-wave field. The E_{hor}-field resonance amplitude is seen to decrease continuously toward the ground. According to the characteristics of a quarter-wave type resonator, B_{hor} minimum and E_{hor} maximum amplitudes at the fundamental frequency are determined at the upper boundary of the resonator (*Prikner and Vagner, 1990*). However, the sharp B_{hor} maximum within the ionospheric F-layer characterizes the position of the horizontal waveguide centre and the shear Alfvén wave resonator appears as *a half-wave type resonator* in the fundamental frequency with the B_{hor}-antinode in the F-layer and nodes above and below the ionosphere (*Lysak, 1999*). The E_{hor}-amplitude is smaller at 20:15 UT than at 19:39 UT, indicating larger wave damping in the IAR during IPDP development. The E_{hor}-ellipticity height profile resembles that of B_{hor}. The a_E-deflection height profile is opposite to a_B-deflection in the main part of the IAR. There are only small differences in the polarization characteristics between the two selected time sections.

Fig. 8 shows the same height profiles as Fig. 6 but for an incident parallel $R_{||}$-mode wave. Comparing Figs. 6 and 8 (at slightly different fundamental resonance frequencies), the normalized B_{hor}-amplitude height profiles are quite similar for $L_{||}$- and $R_{||}$-waves. The $R_{||}$-wave attains a slightly greater total B_{hor}-field amplification in the IAR (a lower damping of the isotropic wave in the ionosphere; see also *Prikner and Vagner, 1983*). An almost circular horizontal polarization is found for the $R_{||}$-wave through the whole height profile above 100 km. The a_B-deflection turns from the magnetic meridian to the NW-SE direction in the main IAR domain below 600 km, i.e. opposite to the $L_{||}$-wave. Below the

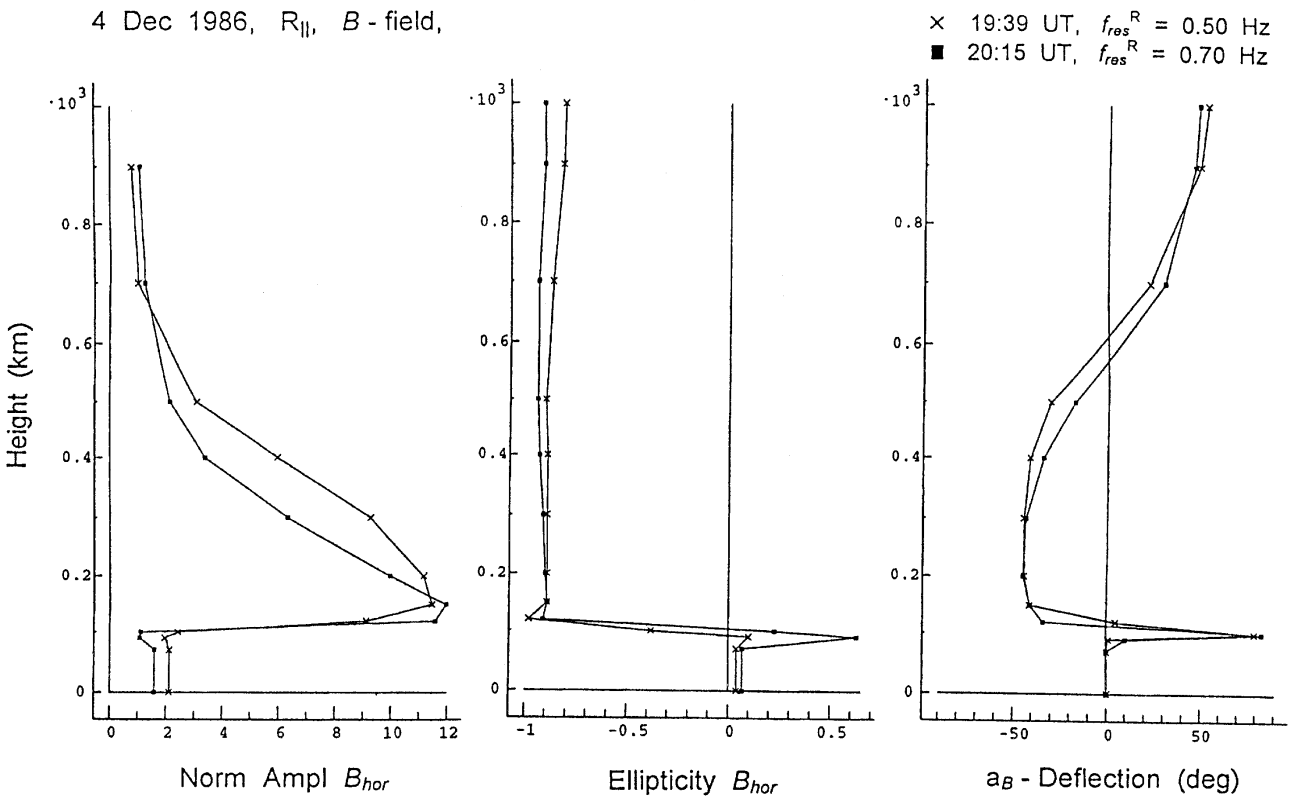

Fig. 8. The same profiles as in Fig. 6, but for the incident $R_{||}$-wave.

E-layer the B_{hor}-amplitude decreases abruptly for both $L_{||}$- and $R_{||}$-mode resonances. There is an altitude zone with a rapid increase of wave damping due to increasing collisions of ions and neutrals, and where the downwards wave energy flux deflects from the magnetic meridian to the horizontal direction (*Prikner et al., 2000*). There are abrupt changes in ellipticity, sense of rotation and a_B-deflection when the wave is transmitted from the ionosphere to the atmosphere.

The highly conductive E-layer is the bottom mirroring layer of the IAR, where numerous wave reflections return waves upwards and contribute to the F-layer B_{hor} maximum. Severe perturbations in the E – region can cause the IAR action to collapse, as mentioned above. Below the neutral atmosphere and on the ground, filtered waves are observed only. However, the B_{hor}-field amplified by the IAR resonance can be observed even there. For the $R_{||}$-wave in Fig. 8 an almost linear polarization with the major axis in the magnetic meridian plane is found from modelling, with a slight dominance of L-sense rotation in the atmosphere and on the ground.

Next we discuss the non-parallel incident waves with L- and R-mode polarization. The incidence angle $\beta = 70°$ in the magnetic meridian plane is assumed (the difference angle $\boldsymbol{k} \wedge \boldsymbol{B}_E$ is 6°). The height profiles of L- and R-waves at 19:39 UT are depicted in Figs. 9 and 10, respectively. As mentioned above, the resonance frequencies are the same as for the parallel incidence. The amplitude profiles show that the B_{hor}-field amplification in the main IAR domain is the same as for the parallel incidence. The profiles of ellipticity show dominant L-sense rotation in the L-wave, and R-sense in the R-wave in the whole main

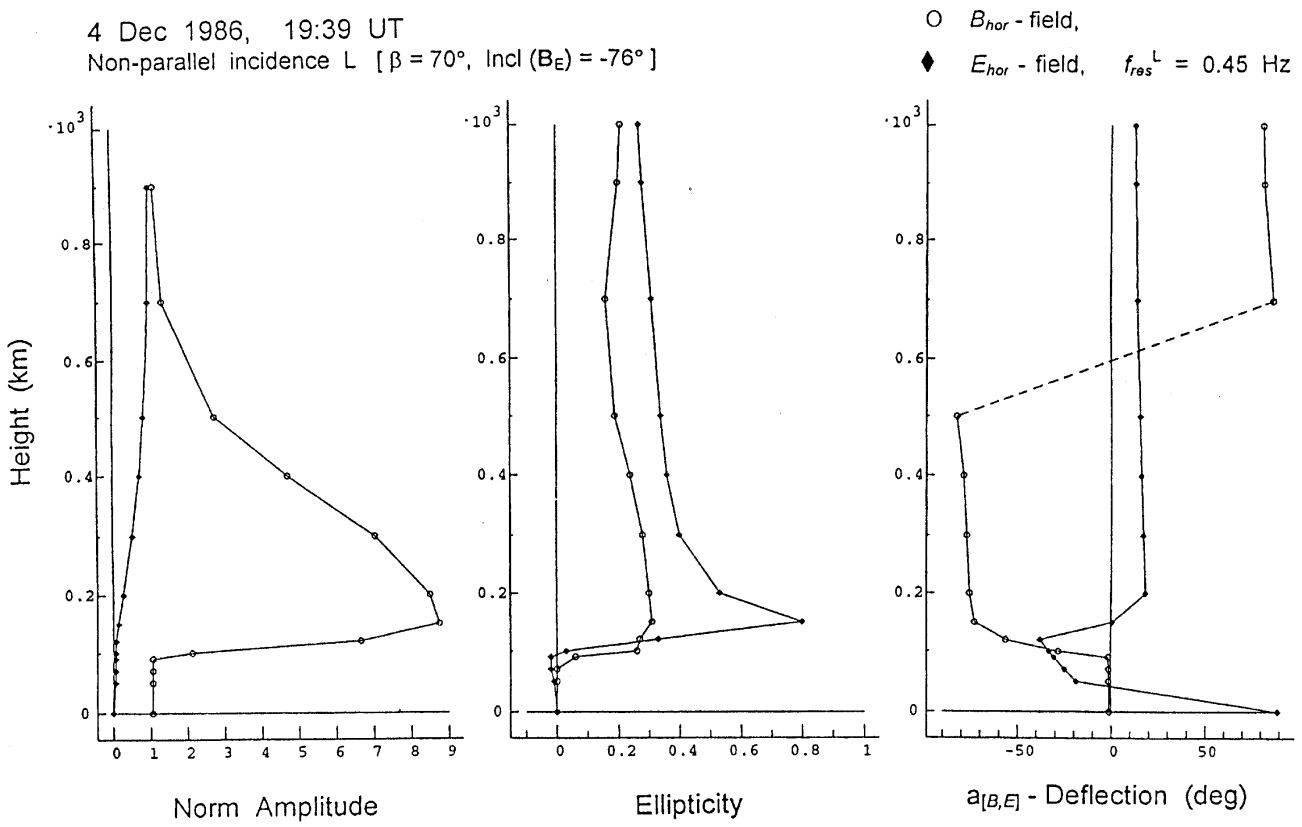

Fig. 9. The height profiles at the fundamental resonance frequency for B_{hor} (marked „o") and E_{hor} (marked by diamonds „◊") amplitudes, polarization ellipticities, and deflections at 19:39 UT for non-parallel incidence of the L-mode wave.

region of the resonator. The polarization ellipses of both L- and R-waves are flatter than for parallel propagation. The a_B- and a_E-deflection characteristics evidently differ for the non-parallel propagation from the parallel one. The B_{hor}-field of the L-wave is oriented nearly perpendicularly to the magnetic meridian plane in the main IAR height domain. For the R-wave, the B_{hor}-field oscillates nearly in the magnetic meridian plane. The polarization of both the L- and R-waves on the ground is roughly linear. However, a more general polarization on the ground can be expected due to the coupling of L- and R-waves when a packet of Pc1 waves with slightly different incidence angles of particular wave-modes penetrates into the IAR.

6. DISCUSSION AND CONCLUSIONS

This paper is a continuation of the study of the non-stationary IAR and its relation to Pc1 and IPDP pulsations. The IPDP formation in the IAR filter, which affects the EMIC waves entering the non-stationary subauroral ionosphere during substorms, was discussed in *Mursula et al. (2000)* and *Prikner et al. (2000)*. The combined effect of substorm-related changes in magnetospheric wave-particle conditions (inward motion of the EMIC wave source, activation of field-aligned currents and particle precipitations), and subauroral ionospheric changes (the trough deepening to lower latitudes) lead to the

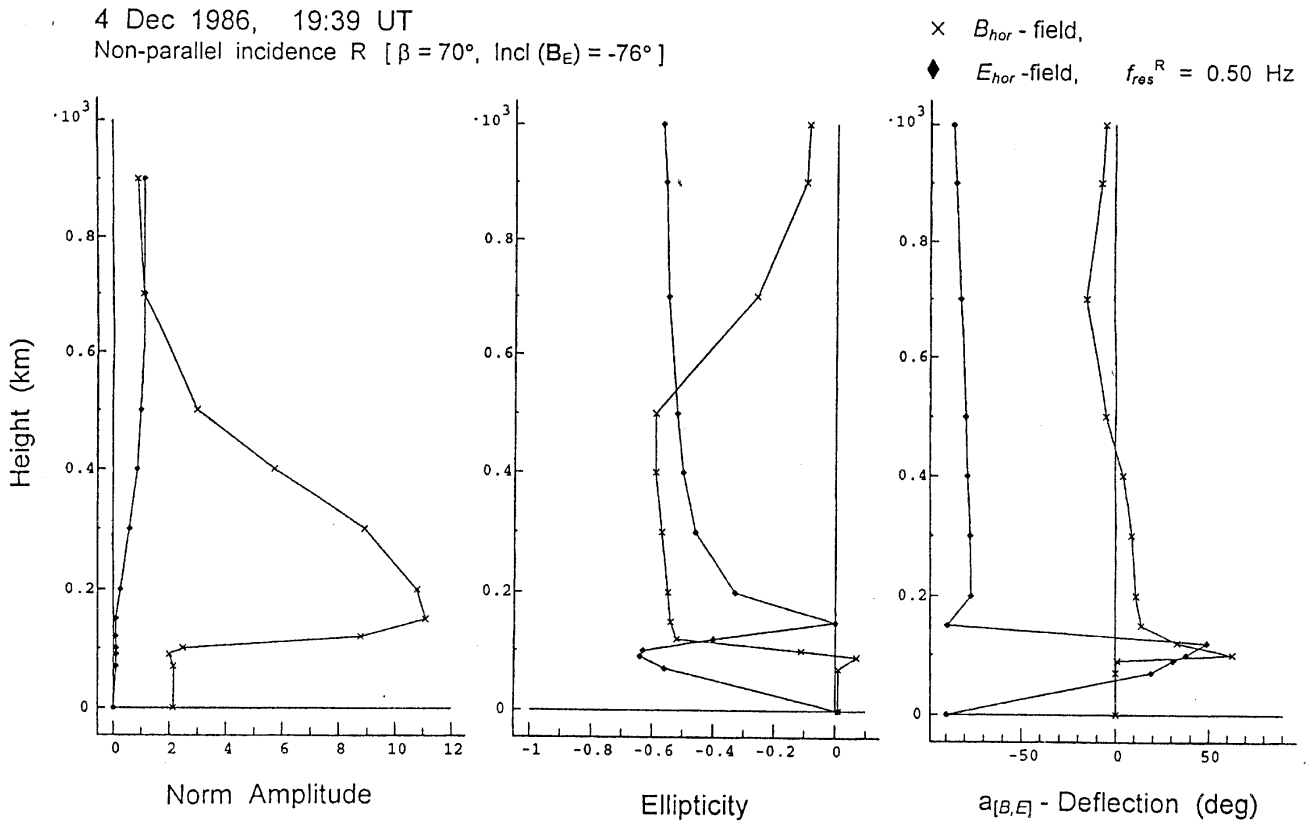

Fig. 10. The same profiles as in Fig. 9 but for an incident non-parallel R-mode wave. (B_{hor}-field marked „×“, and E_{hor}-field „◊“.)

observed IPDP signal on the ground (*Mursula et al., 2000*). An increasing feedback instability of the ionospheric resonance cavity can evoke the latitudinal extension of the trough during a substorm (*Lysak, 1991, 1993*). The increasing fundamental frequency of the IAR must match the EMIC-wave frequency increase during the inward motion of the source. During the substorm onset phase with hot protons precipitating into the ionosphere, considerable perturbations of the lower ionosphere can suppress the IAR action. Simultaneously broad-band signals (PiB-pulsations) can be observed on the ground.

The IAR mechanism has been numerically simulated in a stratified plane ionosphere in an dipole external magnetic field, using a full wave method developed earlier (*Vagner, 1982*; *Prikner and Vagner, 1983, 1991*; *Vagner and Prikner, 1983*). Realistic plasma height profiles have been constructed, based on EISCAT radar measurements of the ionospheric plasma parameters up to 300 km height during the IPDP observation. On the basis of matching both the central frequency of the ground pulsation signal and the simulated IAR fundamental frequency peak an attempt at solving the inverse problem of modelling has been presented in the simple form of extending the $N_e(z)$ profile above the EISCAT measurement range up to 1000 km.

A large resonance amplification of the B_{hor}-wave field in the main IAR domain was specified. During the incidence of the Alfvén wave from the magnetosphere upon the

ionosphere also R-mode waves are generated due to mode coupling. Their part increases especially in the dense ionospheric layers where isotropic modes are able to form compressional waveguide modes propagating in the horizontal direction, transverse to the magnetic field lines (*Greifinger and Greifinger, 1968*; *Altman and Fijalkow, 1980*; *Fujita, 1987*).

In this paper we have illustrated the IAR fundamental frequency height profiles of the total wave characteristics - at different altitudes in the ionosphere and on the ground. Both L- and R- mode wave incidences upon the ionospheric simulation domain, parallel and non-parallel with respect to the external magnetic field line, have been considered. The main results are the following:

a) A large resonance amplification of the B_{hor}-wave field (of the order of 10) was specified in the main IAR region (F-layer) for different incident wave modes corresponding to the situation observed during the IPDP event. Instead, the E_{hor}-wave field was found to decrease monotonously from high to low altitudes in the IAR due to increasing electric conductivity. The vertical profiles of B_{hor} suggest a half-wave type resonator with nodes above and below the ionosphere (see, e.g., *Lysak, 1999*).

b) The ellipticity of oscillation in the horizontal plane is almost circular within the main IAR region for parallel incidence. For non-parallel incidence, the ellipticity decreases (the polarization ellipse flattens) with increasing difference of the incidence angle between $\boldsymbol{k} \wedge \boldsymbol{B}_E$.

c) The B_{hor}- and E_{hor}-wave field oscillations in the main IAR region appear to be nearly perpendicular. For general non-parallel incidence of the L-mode wave (Alfvén wave) the $\boldsymbol{B}$-field oscillates predominantly perpendicular to the magnetic meridian plane and $\boldsymbol{E}$-field parallel to it. For the R-wave the situation is reversed. This effect is less pronounced for parallel incidence due to almost circular polarization.

d) Below the ionosphere and on the ground the simulated total wave horizontal polarization (for a one-mode wave incidence) appears to be practically linear for all the cases of propagation such that the B_{hor}-field is polarized in the plane of the magnetic meridian and the E_{hor}-field perpendicular to it. This is a consequence of the modelling simplification. We restricted ourselves by introducing the approximation characterizing the ground halfspace with the scalar constants of permittivity ε_E and conductivity σ_E instead of frequency-variable tensors $\boldsymbol{\varepsilon}_{\mathbf{E}}(\omega)$ and $\boldsymbol{\sigma}_{\mathbf{E}}(\omega)$, i.e. the homogeneity of the medium has been assumed (*Vagner, 1982*). The assumption of homogeneity entails a spatially limited validity of the mentioned quantities due to possible horizontal inhomogeneities in the Earth's crust. Also the coupling of a fan of particular wave modes (L- and R-, contained in the wave packet) with possibly different incidence angles ($\boldsymbol{k} \wedge \boldsymbol{B}_E$) provides the possibility of a more general polarization on the ground.

e) The calculated instantaneous IAR fundamental frequency peak width corresponded well to the instantaneous IPDP signal frequency spread observed on the ground during the whole wave event. The signal frequency window was permanently located around the IAR fundamental resonance frequency peak.

Acknowledgements. J. K., R. K., and K. M. gratefully acknowledge the financial support by the Academy of Finland. F. Z. F. gratefully acknowledges the financial support by the Commission of the European Union (Brussels) through Research Grant INTAS 99-0335, and the finantial support of the Russian Fund of Basic Research (grants 02-05-64610 and 02-05-64612). K. P. thanks T. Pikkarainen for the magnetic data and P. Pollari for the EISCAT data.

The EISCAT Scientific Association is supported by the Suomen Akatemia of Finland, Centre National de la Recherche Scientifique, France, Max-Planck Gesellschaft, Federal Republic of Germany, National Institute of Polar Research of Japan, Norges Almenvitenskapelige Forskningsrad of Norway, Naturvetenskapliga Forskningsradet of Sweden, and the Science and Engineering Research Council of the United Kingdom.

Received: October 8 2001; *Accepted: February 21 2002*

References

Altman C. and Fijalkow E., 1980. The horizontal propagation of Pc1 pulsations in the ionosphere. *Planet. Space Sci.,* **28,** 61-68.

Bauske R., Noel S., and Prölss G.W., 1997. Ionospheric storm effects in the nighttime E region caused by neutralized ring current particles. *Ann. Geophysicae,* **15,** 300-305.

Belyaev P.P., Bösinger T., Isaev S.V., Trakhtengerts V.Y. and Kangas J., 1999. First evidence at high latitudes for the ionospheric Alfvén resonator. *J. Geophys. Res.,* **104,** 4305-4317.

Belyaev P.P., Polyakov S.V., Rapoport V.O. and Trakhtengerts V.Y., 1985. Characteristics of wave generation in an asymmetrical Alfvén maser. *Geomagn. Aeron.,* **25,** 502-504.

Belyaev P.P., Polyakov S.V., Rapoport V.O. and Trakhtengerts V.Y., 1989. Experimental studies of the spectral resonance structure of the atmospheric electromagnetic noise background within the range of short-period geomagnetic pulsations. *Radiophizika,* **32,** 663-672.

Belyaev P.P., Polyakov S.V., Rapoport V.O. and Trakhtengerts V.Y., 1990. The ionospheric Alfvén resonator. *J. Atm. Terr. Phys.,* **52,** 781-788.

Demekhov A.G., Trakhtengerts V.Y., Polyakov S.V., Belyaev P.P. and Rapoport V.O., 1994. An Alfvén sweep maser model for Pc1 pearls: theory. In: *NIRFI's preprints,* pp. 1-26, NIRFI, Nizhny Novgorod, Russia.

Demekhov A.G., Belyaev P.P., Isaev S.V., Manninen J., Turunen T. and Kangas J., 2000. Modelling the diurnal evolution of the resonance spectral structure of the atmospheric noise background in the Pc frequency range. *J. Atmos. Sol.-Terr. Phys.,* **62,** 257-265.

Fujita S., 1987. Duct propagation of a short-period hydromagnetic wave based on the international reference ionosphere model. *Planet. Space Sci.,* **35,** 91-103.

Greifinger C. and Greifinger P., 1968. Theory of hydromagnetic propagation in the ionospheric wave guide. *J. Geophys. Res.,* **73,** 7473-7490.

Gul'elmi A.V., 1974. Diagnostics of the magnetosphere and interplanetary medium by means of pulsations. *Space Sci. Rev.,* **16,** 331-345.

Heacock R.R., 1973. Type IPDP magnetospheric plasma wave events. *Nature Phys. Science,* **246,** 93-96.

Hughes W.J., 1974. The effect of the atmosphere and ionosphere on long period magnetospheric micropulsations. *Planet. Space Sci.,* **22,** 1157-1172.

Kangas J., Aikio A. and Pikkarainen T., 1988. Radar electric field measurements during an IPDP plasma wave event. *Planet. Space Sci.,* **36,** 1103-1109.

Kangas J., Lukkari L. and Heacock R.R., 1974. On the westward expansion of substorm - correlated particle phenomena. *J. Geophys. Res.,* **79,** 3207-3210.

Kleimenova N.G., Kangas J., Pikkarainen T. and Ranta C., 1995. The geomagnetic pulsations IPDP and the main ionospheric trough (in Russian). *Geomagn. Aeron.,* **35,** 60-68.

Koleszar T.W., 1989. *The generation of IPDP micropulsations, with special attention to frequency shift mechanisms.* Ph.D. thesis, The University of British Columbia (Canada).

Krinberg I.A. and Taschilin A.V., 1984. *The ionosphere and the plasmasphere* (in Russian). Nauka, Moscow.

Lysak R.L., 1991. Feedback instability of the ionospheric resonant cavity. *J. Geophys. Res.,* **96,** 1553-1568.

Lysak R.L., 1993. Generalized model of the ionospheric Alfvén resonator. *Auroral Plasma Dynamics, Geophysical Monograph* **80,** 121-128, Copyright by the American Geophysical Union.

Lysak R.L., 1999. Propagation of Alfvén waves through the ionosphere: dependance on ionospheric parameters. *J. Geophys. Res.,* **104** (A5), 10117-10030.

Mursula K., Prikner K., Feygin F.Z., Bräysy T., Kangas J., Kerttula R., Pollari P., Pikkarainen T. and Pokhotelov O.A., 2000. Non-stationary Alfvén resonator: new results on Pc1 pearls and IPDP events. *J. Atmos. Sol.-Terr. Phys.,***62,** 299-309.

Nishida A., 1964. Ionospheric screening effect and storm sudden commencement. *J. Geophys. Res.,* **69,** 1861-1874.

Polyakov S.V. and Rapoport V.O., 1981. Ionospheric Alfvén resonator. *Geomagn. Aeron.,* **21,** 610-614.

Prikner K., 1986. The ionosphere of higher geomagnetic latitudes (L = 3 and L = 5) as a ULF wave filter. *Studia geoph. et geod.,* **30,** 304-319.

Prikner K., Feygin F.Z. and Fligel D.S., 1996. Determination of the electron concentration profile of the ionospheric Alfvén resonator after spectral structure of series of the geomagnetic Pc1 pulsations (in Russian). *Geomagn. Aeron.,* **36,** 62-69.

Prikner K., Mursula K., Feygin F.Z., Kangas J., Kerttula R., Pikkarainen T., Pokhotelov O.A. and Vagner V., 2000. Non-stationary Alfvén resonator: vertical profiles of wave characteristics. *J. Atmos. Sol.-Terr. Phys.,* **62,** 311-322.

Prikner K., Mursula K., Kangas J. and Feygin F.Z., 2001. Ionospheric Alfvén resonator control over the frequency-variable Pc1 event in Finland on May 14, 1997. *Studia geoph. et geod.,* **45**, 363-381.

Prikner K. and Vagner V., 1983. Numerical modelling of the ionospheric filtration of an ULF micropulsation signal. *Studia geoph. et geod.,* **27,** 173-190.

Prikner K. and Vagner V., 1990. The ionosphere as an Alfven resonator in the Pc1 micropulsation range. *Studia geoph. et geod.,* **34,** 342-361.

Prikner K. and Vagner V., 1991. Numerical solution to the problem of ionospheric filtration of ULF waves in the Pc1 range. The total wave field inside the ionospheric transition layer. *Studia geoph. et geod.,* **35,** 90-99.

Trakhtengerts V.Y., Demekhov A.G., Polyakov S.V., Belyaev P.P. and Rapoport V.O., 2000. A mechanism of Pc1pearl formation based on the Alfvén sweep maser. *J. Atmos. Sol.-Terr. Phys.,* **62,** 231-238.

Vagner V., 1982. Numerical solution of ionospheric filtration of ULF waves (Part I - Method). *Travaux Géophysiques,* **XXX** (No 576), 199-229.

Vagner V. and Prikner K., 1983. Polarization characteristics of ionospheric filtration of ULF waves. *Studia geoph. et geod.,* **27,** 285-297.